Point Ahead Mechanism for Deep Space Optical Communication Development of a New Piezo-Based Fine Steering Mirror

Adrien Guignabert*, Thomas Maillard*, Francois Barillot*, Olivier Sosnicki* and Frank Claeyssen*

Abstract

The purpose of this paper is to present the development of a novel tip-tilt mechanism, with integrated optics, designed for the JPL Deep Space Optical Communication (DSOC) module of the upcoming Psyche mission (2022 launch). This paper presents the design, assembly and tests of the produced models. Regarding the design phase, an emphasis was put on the mirror calculations to ensure that the required flatness would be maintained after integration, and that the part would withstand the thermal/mechanical environment. The actual optical measurements performed after assembly are also presented. The qualification results for a new alpha-case removal process for titanium parts are presented. Tests results are especially interesting regarding the temperature behavior of the mechanism, impact on the stroke, and strain gage sensor feedback.

Introduction

In the upcoming NASA Psyche mission (2022 launch), JPL is planning the assessment of a first Deep Space Optical Communication (DSOC) module. In this module, a Point Ahead Mechanism (PAM) aims at steering the optical downlink signal towards anticipated earth position during DSOC communication phases.

As a background, for 20 years, Cedrat Technologies (CTEC) has provided various piezoelectrically-actuated Beam Steering Mirrors as well as Fast Steering Mirrors for space missions (PHARAO for CNES, ATLID for Airbus DS) as well as for optronic equipment in defense [1-5]. More recently, CTEC has also been active in Free Space Optical Communication with a new large-stroke Fast Steering Mirror [4].

In this context, CTEC was subcontracted by L3Harris, to design, manufacture and test the performance of the PAM engineering and flight models for JPL PSYCHE DSOC. The developed PAM is a new tip-tilt mechanism based on low-voltage Amplified Piezoelectric Actuators (APA®), exploiting its space heritage.

This paper presents the design, assembly and tests of the produced PAM models, covering the involved technologies and failure modes: piezo materials for actuation, strain gages for indirect angular position sensing, mechanical parts treatments, tip-tilt mechanical structure, mirror flatness, etc.

Mechanism Design

Specifications and Timeline

The main specifications for this mechanism were to ensure an angular stroke of ±2,8 mrad throughout the full operational temperature range of the mission (-25/+50°C full perf, -40/+65°C reduced perf) and a mirror surface flatness under 63 nm while remaining inside a very limited volume and surviving launch vibrations.

The project really started in summer 2018 with a preliminary feasibility study aimed at validating these specifications, which ended positively in Fall 2018. The initial design was first based on ATLID mechanism but specific requirements made it progressively, noticeably different in the end. The required schedule for the final mechanism development, i.e,. delivering Flight models less than 1 year after the actual project start, was very unusual and challenging.

* Cedrat Technologies, Meylan, France; Adrien.guignabert@cedrat-tec.com

Mechanism Overview

The piezo actuators are wired in 2 push-pull configurations (1 per axis) to allow direct mirror rotation control. The PAM itself is composed of the following parts:

- A bracket baseplate (in aluminum): The APA® are fixed on it with screws.
- 4 APA® (in titanium): They provide the required displacement and are fixed to the baseplate and to the mirror support via flexural pivots. The APA® are equipped with Strain Gauge (SG) sensors that are bonded in place
- 4 circular pivots (in titanium).
- A mirror support (in INVAR) which holds the mirror.
- A guiding blade (in titanium) soldered onto the central cylinder that stiffens the assembly.
- A Silicon Carbide (SiC) substrate-based mirror from Mersen OptoSiC®

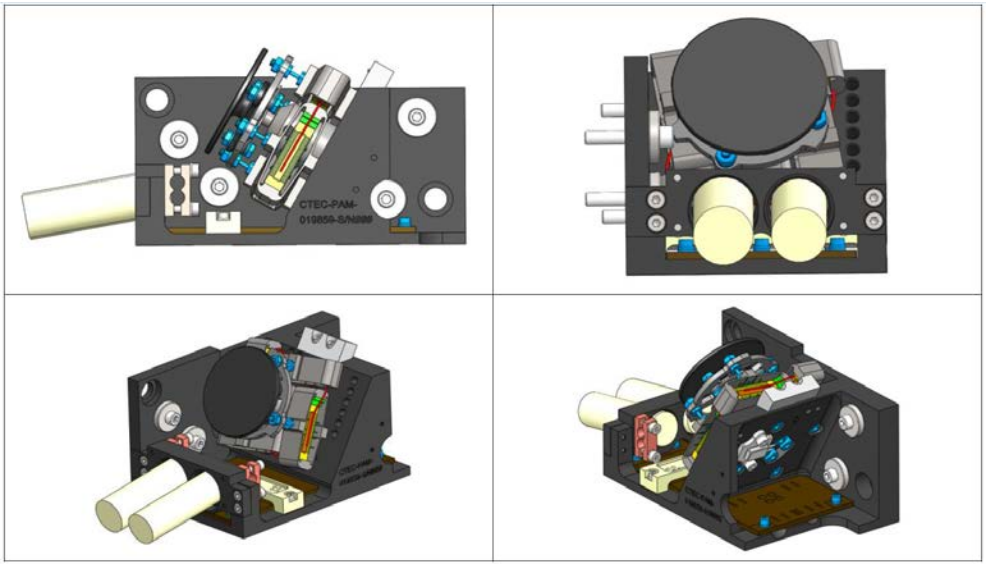

Figure 1. PAM Overview Including Piezo and Optical Technology from Cedrat Technologies

Strain Gauge Sensing

In order to be able to monitor the mirror angle, an indirect solution using strain gages placed on each piezo actuator is selected, based on space heritage from other projects, especially ATLID on this matter, which enabled an important development on SG assembly process. The initial SG redundancy requirement was lifted, because it required an important wiring complexity (32 instead of 16 wires), amongst other additional constraints.

The project used constantan, 350-ohm SG. There are 2 SG per piezo stack, mounted in one full Wheatstone bridge per rotation axis to maximize the sensitivity while minimizing thermal drift. All SG wires and printed circuit board (PCB) traces are the same length to limit offset drift.

New Piezo Actuator Design

The existing CTEC actuators were either slightly too short in stroke or not stiff enough to ensure the mechanism survival during launch. The mechanism consists of 4 APA®, derived from CTEC standard APA120S but specifically designed for the application needs.

Based on CTEC space heritage, the APA® shell was made from Ti6Al4V titanium, allowing a theoretical infinite fatigue lifetime in the specified operational conditions and an interesting stiffness/mass ratio. Another benefit of the use of titanium rather than steel as used in standard products, is the reduction of the thermal stroke effect due to a better CTE match (9 ppm/K) to the piezo stack (typically -3 to +1ppm/K) compared to a high performance stainless steel for example (10-11 ppm/K). A total of 18 APA® were assembled and tested, the results are indicated in Table 1.

Table 1. PAM Actuators Measured Results

	Full stroke (170 V pp)	**1st coupled resonant frequency**
	µm	Hz
Average measured	149.2	6963.6
Standard deviation measured	2.0	60.9
Design value (worst case)	130.4	6151
Difference measurement/design value	14%	13%

The design values are based on expected worst case parameters, i.e., low piezo gain and stiffest shell when calculating the stroke. A conservative approach was used to ensure that the required mechanism stroke would always be reached, which resulted in average margins of 14% for the stoke and 13% for 1st resonant frequency.

Integrated Optics – Mirror Development

The PAM is designed around one of its core components: the mirror. For this new project, CTEC used its experience on piezo-optical aerospace projects and collaborated with partners in order to fully integrate the optical hardware development, from the SiC mirror design to its integration and optical verifications.

Mirror design

One of the main design constraints of an embedded optics mechanism is to keep the mirror surface deformation to a minimum in order to limit the induced optical wave front error below the requirements. In this case, a maximum of 63-nm mirror surface flatness is the requirement. In order to ensure the specification would be reached, CTEC developed tools and performed specific simulations in the early design phase, specifically including verification of induced surface figure error caused by mechanical biases and thermal deformation, as well as optimization of mirror shape and dimensions.

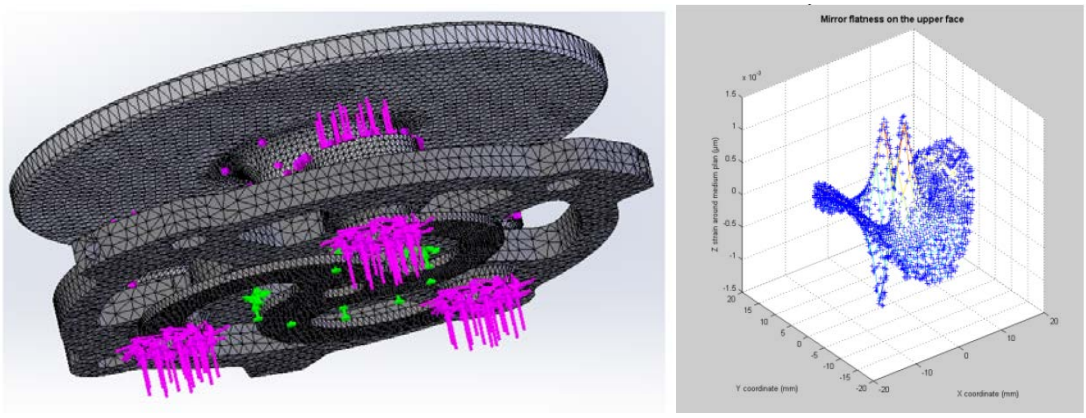

Figure 2. Mirror Surface Deformation Simulation Meshing and Boundary Conditions (Screw Tension and Torque Case) (Left) - Mirror Surface Deformation Evaluation Results (Right)

The mirror design process is based on a finite element simulation of each mirror deformation contributor: mirror clamping to its support, actuator height variation, screw tightening and thermal operational. Each case used representative boundary conditions. The resulting displacement on each of the mirror surface points is then exported. A MATLAB program is then run to post process the results from the simulation. Extracting the RMS reference plane from this data set, it calculates the distance of each point to this plane, the peaks and valley of the deformed mirror and the resulting RMS deformation. The specific contribution of each evaluated case on the mirror deformation is then summed up to give an estimation of the total expected mirror surface deformation.

PAM development also included a regular mirror optical verification at different stages of the assembly, with the intention of having the ability to stop the process should a mirror appear to be out of the acceptable range or show significant surface figure changes from one step to another. With the recent CTEC experience on this matter, such regular controls also allowed us to learn a lot regarding the impact of each assembly step as well as providing a safer project assembly process.

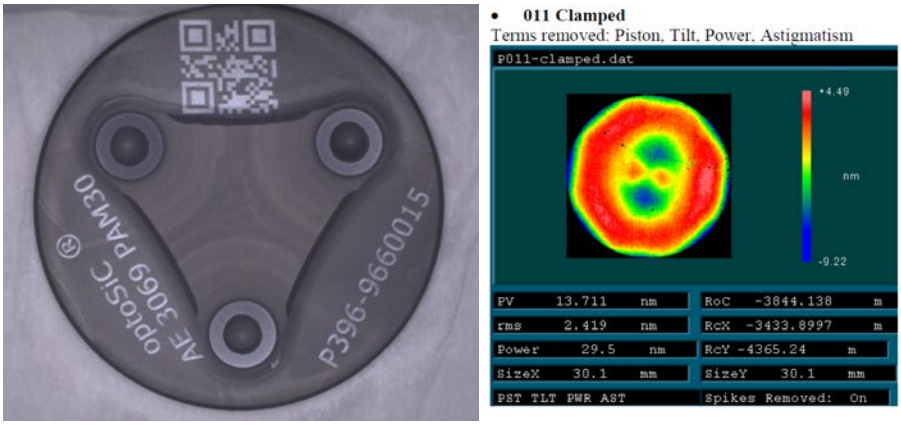

Figure 3. Mirror interface (left) and surface verification with interferometer (right)

Mirror Verification Results

A total of 4 PAM were produced and the mirror Reflected Wavefront Error, Peak-to-Valley (RWE PV, basically 2 times mirror surface flatness error SFE) was measured in different phases, i.e., mirror in the initial free condition, once clamped on its mount, and eventually after final integration in mechanism.

Table 2. PAM Mirror Surface Flatness Measurement Results

PAM model	**1.Free coated mirror**		**2.Mirror clamped on mount**		**3.Mirror integrated in final mechanism**		**Calculation: Mechanism contribution to mirror deformation**	
	RWE PV (nm)	RWE RMS (nm)	RWE PV (nm)	RWE RMS (nm)	RWE PV (nm)	RWE RMS (nm)	RWE PV (nm)	RWE RMS (nm)
EM	38.1	10.1	34.9	8.9	41.3	10.6	3.2	0.5
EQM	22.2	6.2	27.2	6.6	38.7	10.3	16.5	4.1
FM1	23.2	5.5	19.4	4.6	26.6	6.0	3.4	0.5
FM2	28.9	8.1	33.8	8.2	34.1	9.5	5.2	1.4
Average	28.1	7.5	28.8	7.1	35.2	9.1	7.1	1.6

With an average 35.2 nm and a maximum of 41.3 RWE PV, the <127-nm RWE specification was reached with significant margin. The last column evaluates the proper mechanism contribution to mirror deformation based on the difference between final and the initial RWE PV measurements.

The mechanism average contribution to the mirror deformation appears to be limited to 7.1 nm PV and 1.6 nm RMS.

Eventually, we can compare these results to the expected worst-case deformations evaluated during the design phase. The thermomechanical contribution could not be evaluated so only mechanism induced deformation are considered.

Table 3. Comparison of mirror measurements and expected design worst cases

	Average measured impact of mechanism on mirror RWE (nm)	**Average measured impact of mechanism on mirror SFE (nm)**	**Evaluated worst case for mirror SFE (mechanism integration only) (nm)**
PV	7.1	3.5	5.7
RMS	1.6	0.8	3.1

All measured values are within the expected range of mirror deformation, indicating that the conservative simulation approach was correct in that case.

Mechanism Production and Assembly

Titanium Parts – Alpha Case Removal Process Qualification

The use of titanium for some parts, justified by its interesting mechanical properties and heritage on previous CTEC mechanisms (for similar parts) is not without drawbacks. The main issue is due to the use of wire electro discharge machining (WEDM) for the “flexible” parts manufacturing, i.e., the actuator amplification shell and the guiding blade at the center of the mechanism. This manufacturing technique is required due to the parts geometry.

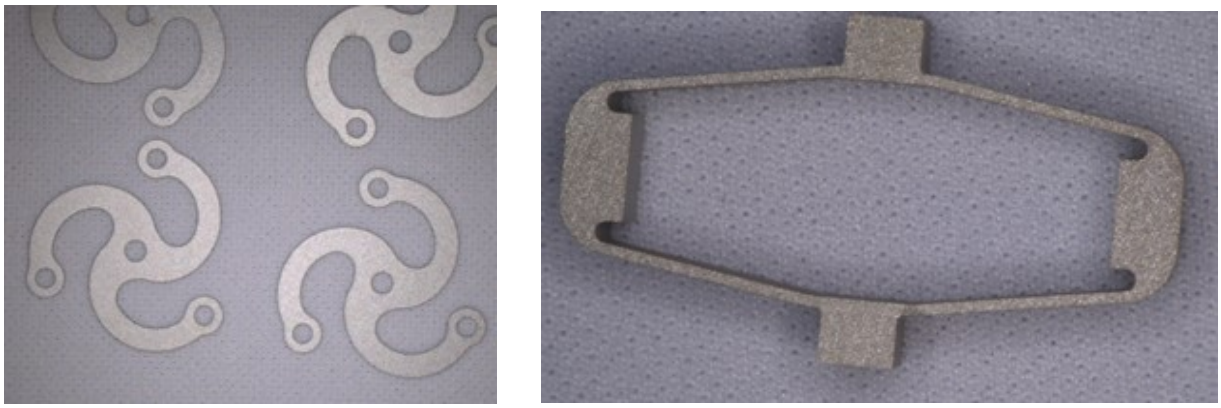

Figure 4. WEDM titanium parts, guiding blade (left) and actuator shell (right), different scale

The WEDM locally heats the material which can induce the formation of an alpha case on the surface, with the adverse effect of lifetime reduction (up to 30% according to [6]), and possibly unexpected failures. This alpha case, usually a few µm thick, can be removed through proper chemical etching.

For this mechanism, the already qualified manufacturer was not compatible with the required schedule (overload), hence a backup option had to be identified and qualified. The new supplier proposed an acid etching process. The qualification process was the following:

- Machine a set of guiding blade and actuator shell, identical to flight design (supplier, process, material batch, dimensions)
- Perform an alpha case analysis before acid etching, parts in initial state, as well as an interstitial hydrogen contamination measurement.
- Pass the parts through the acid etching process, adjusted to remove the required thickness
- Perform an analysis after the chemical etching: alpha case and interstitial hydrogen contamination
- The process is qualified if analyses show no trace of alpha case after etching and no more than 150 ppm interstitial hydrogen contamination.

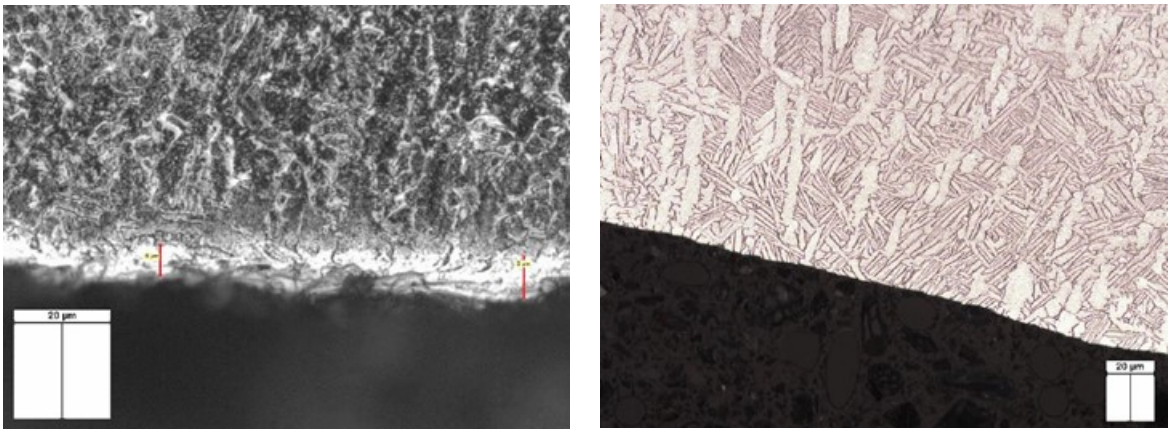

Figure 4. Alpha Case Analysis, Before (Left) and After the Acid Etching (Right)-Optical Microscope (x1000)

No alpha case was found on that actuator shells; on the guiding blade however, the average alpha case thickness was 8 µm (6 to 11 µm). It was decided that a 15-µm thickness removal through acid etching would be enough to remove the alpha case.

The final analysis after the acid etching indicates that the process efficiently removed the alpha case (see Figure 4), no trace was left on the part. The hydrogen contamination, that can be induced during the acid etching (penetration of hydrogen inside the material compound and local embrittlement) remained within the boundaries (86 ppm for guiding blade and 26 ppm for actuator shells). The process is then qualified and was used successfully to treat flight parts.

Piezoelectric Stacks – Lot Acceptance Tests (LAT)

As one of the critical items in the mechanism (brittle, sensitive part), the piezo stacks are handled with special care. One single piezo batch is procured for the project, with high quantity margin (at least x2). An LAT is then performed on 4 piezo stacks taken from this batch, prepared (SG gluing & cabling) exactly as flight piezos.

This LAT includes thermal cycling and lifetime tests representative to the final environment (this includes mounting them in their actuator shell). Regular basic electrical verifications (capacitance, insulation), stroke measurements are performed before and after the tests to detect any deviation. A final destructive physical analysis is performed to inspect inner features of the piezo stacks mainly to detect potential voids in the ceramic and electrode delamination. Piezo stacks are cut in two and sections are inspected.

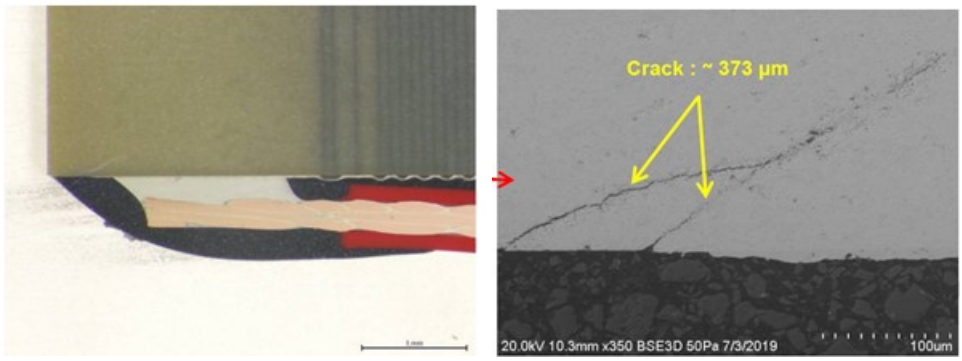

Figure 5. Solder Inspection, Example of a Crack

The destructive physical analysis revealed that the material is dense enough, no voids were detected. Electrodes were perfectly in place and no trace of delamination was found. In compliance with CTEC

previous experience, small 45° cracks were detected in the vicinity of the electrodes. These cracks are believed to be caused by the thermal expansion and contraction of the electrode during soldering. Since they are covered in epoxy potting, the cracks' progression is contained.

However, one unusually placed and lengthy crack was detected. Unusual by its location, starting from piezo edge instead of from the electrode, and by its length, 2.2 mm compared to the usual few hundred µm.

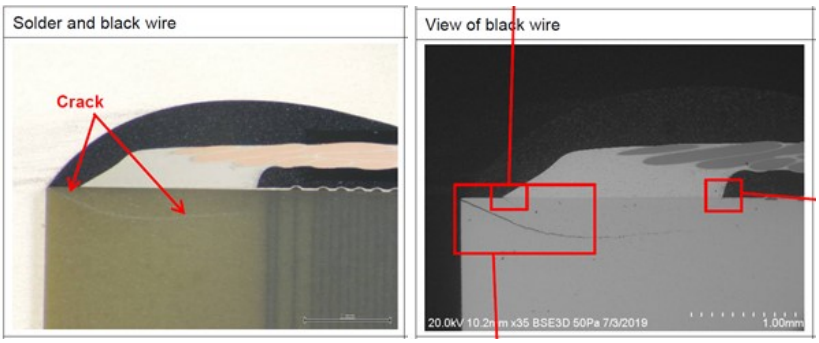

Figure 6. Piezo N°3, Black Wire Side Unusual Crack (Length 2.2 mm)

Raising questions, investigations were performed but no clear specific root cause was identified. It was found that this crack was slightly visible from the exterior and most importantly not going through the entire stack (staying near the electrode, under the epoxy).

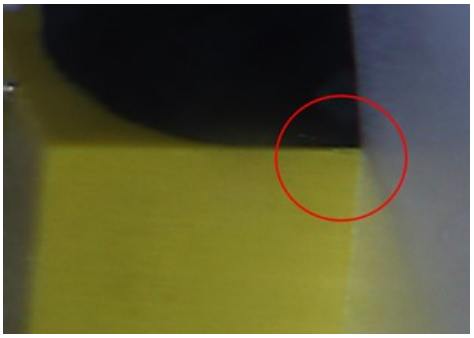

Figure 7. Exterior View of the Crack

One possible root cause for this crack is stress concentration due to a slight mispositioning inside the actuator shell and to the selected prestress level. Simulations representing this mispositioning allowed CTEC to map the induced stress concentration and the result is visually similar to the observed crack pattern.

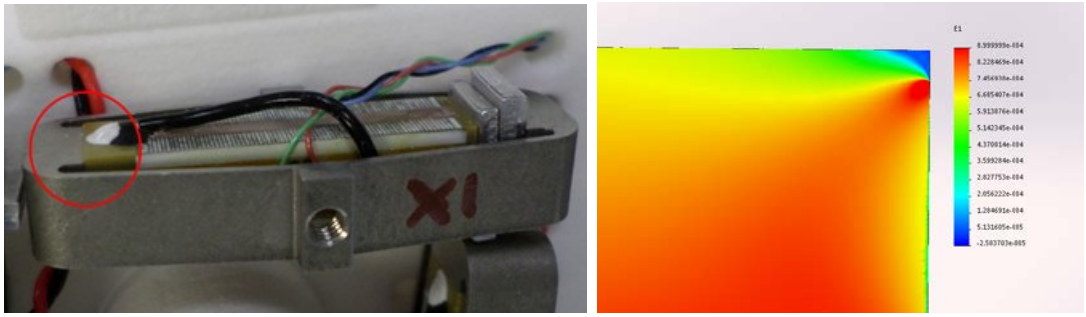

Figure 1. Photo of Piezo Mispositioning and Simulation of Corresponding Principal Deformation Map (Cut View) Matching Crack Pattern

To avoid this problem, the final flight actuator shell will be larger (9 mm instead of 5 mm) than the one used for the LAT, making it impossible for the piezo face to be in contact with an edge like this. Also, as a precaution, all piezo stacks were inspected before assembly in flight hardware and no exterior sign of similar cracking was found.

No other unusual findings were identified, and the piezo batch was accepted for integration.

Mechanism Integration

One of the main constraints of this mechanism integration is that the support bracket (black anodized aluminum part) has its interface surface (fixed to the L3 optical array) perpendicular to the mechanism base plane. This geometry severely limits access to the mechanism for torque wrenches, operator hands, pliers etc. Hence the assembly process had to integrate this specific constraint with the unusual approach to pre-assemble the actuation mechanism outside its final base plate, then transferring it onto the final support bracket. The final mechanism once assembled is shown in Figure 9.

Figure 9. PAM EQM Picture After Assembly

The most sensitive part of the mechanism is its SiC coated mirror and many precautions were taken to protect it during the assembly. A specific cover (POM-C) was designed and was used for most assembly phases, especially to protect the mirror surface from wrenches or pliers when needed. In order to ensure additional protection during transportations phases (models are transported several times during assembly and test phases), a transparent Plexiglas box was designed.

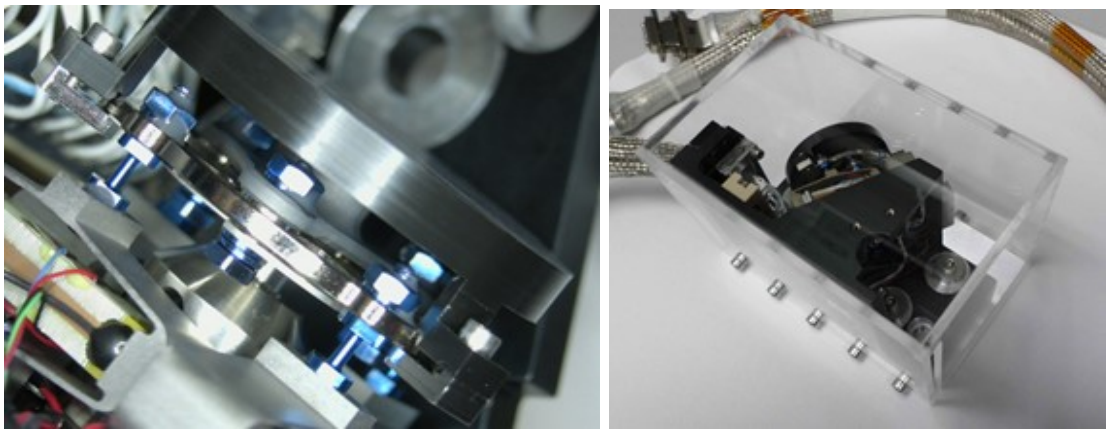

Figure 10. Mirror Protection Cover Once Installed (Black Part), PAM Transportation Box

Cables and PCB Integration

A total of 16 SG sensor wires and 8 piezo power wires have to be routed from the mechanism to the interface cables. The use of a connector on the PAM side was not possible due to size constraints. The selected design option was an interconnection PCB, similar to what was used in previous CTEC space mechanisms like the ATLID Beam Steering Mirrors(1). The multilayer PCB provides many benefits:

- Allows pre-routing of all SG bridges easily
- Easier wire handling and more reliable interconnection (from AWG36 SG wires to AWG26 pigtail cable wire, large number of wires)
- More control of SG trace length (and impedance) to ensure a reduction of SG offset thermal drift
- SG and piezo signals are routed through different layers, insulated and shielded from each other (ground planes in the middle of the PCB)
- Interconnection PCB was used in previous similar space projects with positive feedback

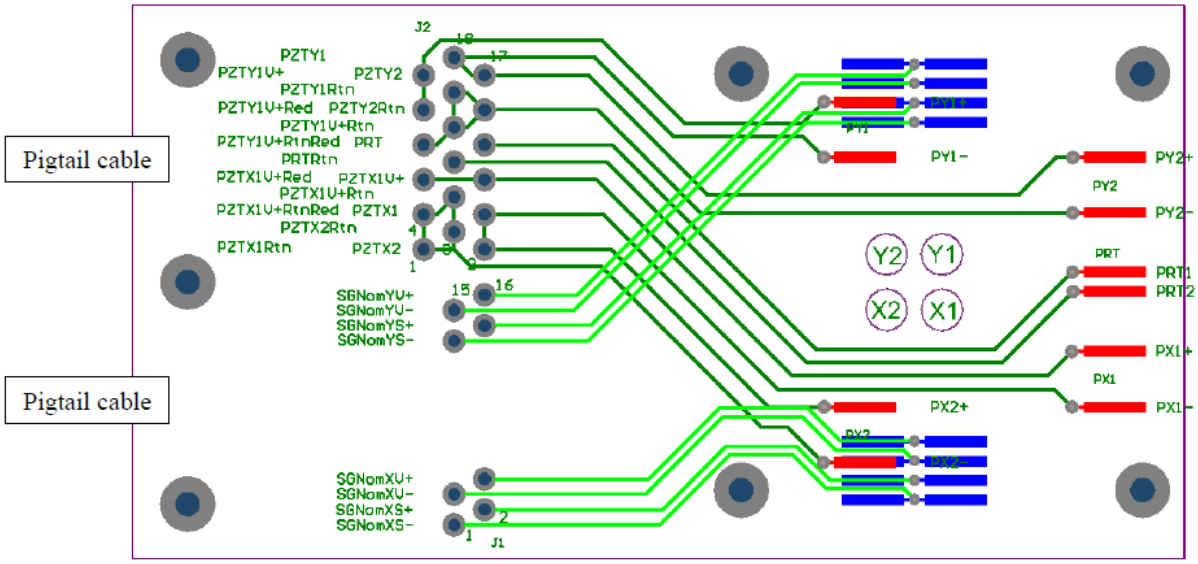

Figure 11. PAM PCB routing overview (merged layers for easier visualization)

Wires are routed from their starting point on the piezo actuators (SG and power), through the support bracket via holes, up to their dedicated PCB pad. Wires are regularly secured along their paths with epoxy dots. One of the constraints of SG wire is for them to have the same length within each Wheatstone bridge (one for each axis) to ensure they maintain the same total resistance within the target range.

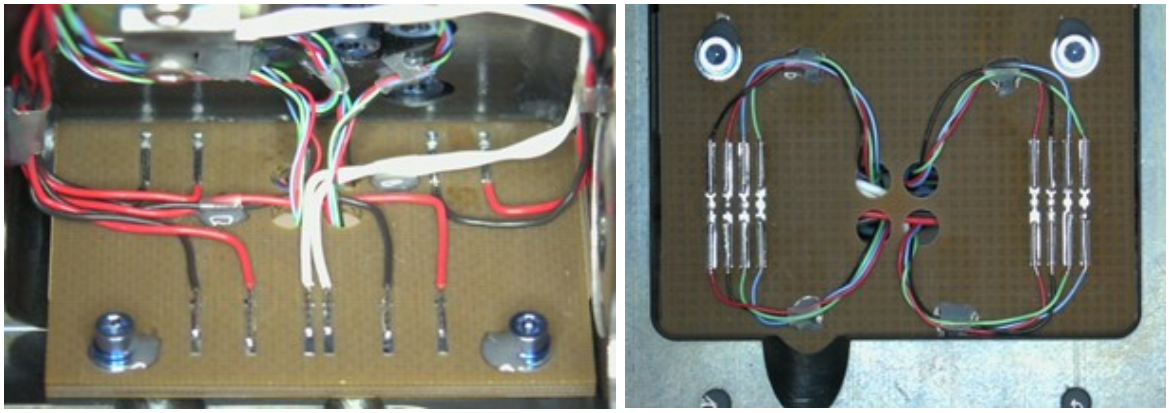

Figure 12. PAM Cabling to Interconnection PCB

Static Performance

The 4 mechanism performance parameters are verified at different steps of their acceptance tests. An initial good health verification was also performed to ensure that the piezos and SG were correctly cabled. At the time of this paper publication, only 3 mechanisms were tested, results are presented in Table 4.

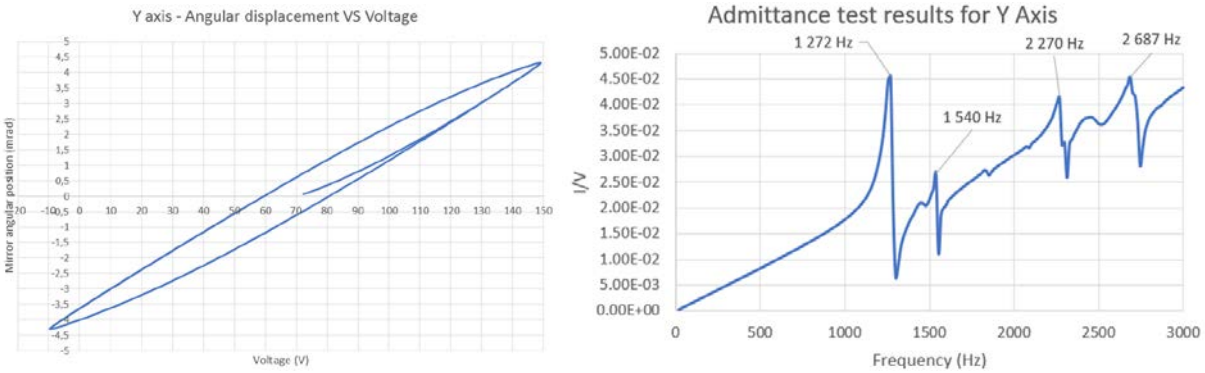

Figure 13. EQM Y Axis Full Stroke Measurement (Mirror Angle vs Push-Pull Voltage) and Admittance Sweep for EQM Y axis – Coupled Resonance Frequency Identification

Table 4. Static Measurement Results for PAM EM/EQM and FM2

Parameter	Required value	EM	EQM	FM2
PAM total stroke at ambient (-10/+150V)				
X axis	>6 mrad	8.0 mrad	8.7 mrad	8.5 mrad
Y axis	>6 mrad	8.6 mrad	8.6 mrad	8.5 mrad
SG response at ambient- Functional tests FTM-01-B (cf, III,8)				
Offset				
X axis	/	-0.71 mrad	-0.27 mrad	-0.46 mrad
Y axis	/	-0.76 mrad	-0.35 mrad	0.11 mrad
Gain				
X axis	/	1.57 mrad/V	1.49 mrad/V	1.76 mrad/V
Y axis	/	1.38 mrad/V	1.54 mrad/V	1.67 mrad/V
1st coupled resonance frequency				
X axis	>800Hz	1495 Hz	1301 Hz	1257 Hz
Y axis	>800Hz	1242 Hz	1272 Hz	1272 Hz
PAM mass				
Total mass	/	497.2 g	497.9 g	495.1 g

The mechanism total stroke is compliant with the specification with significant margin, since design anticipated some stroke loss at cold temperature. The total stroke is similar for all models/axes, the slight variation observed is expected and linked to the piezo actuators' stroke/stiffness variation.

SG parameters are noted for information, only the variation of these parameters (over temperature) matters. Note that SG measurements are taken after bridge output conditioning (5V excitation, 337 and 352 V/V gain for X and Y).

Thermal Vacuum Testing

The Qualification campaign for the EQM included both non-operational (NOP) and operational (OP) thermal vacuum cycling. Target vacuum is <10-5 mbar. Tests A,B,C are functional tests (stroke, SG and admittance sweep).

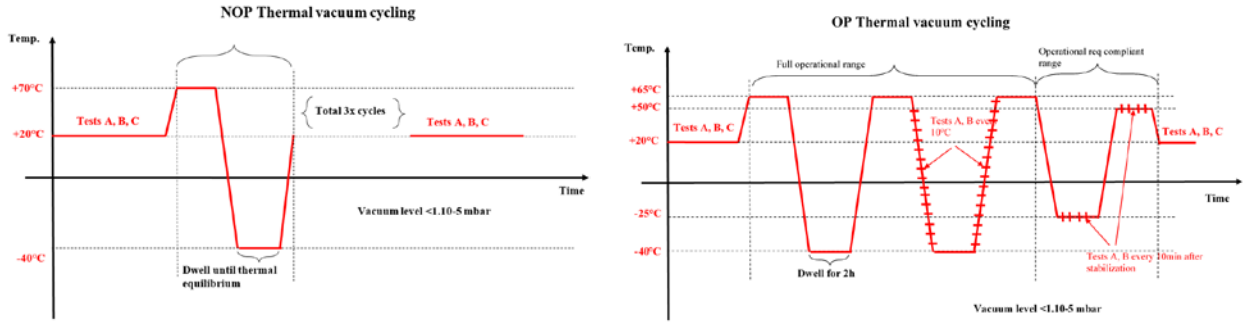

Figure 14. NOP and OP Thermal Vacuum Cycling Test Schematic

The main objective of the OP Thermal Vacuum Cycle is to characterize the variation of PAM stroke (expected loss in cold) and SG performance throughout the OP temperature range. Only the results of this test are detailed in this paper. The OP Thermal Vacuum Cycle consists of testing the mechanism (full stroke, SG parameters) at different incremental temperatures (every 10°C).

Given that the PAM applied voltage was not constant during the full test (4 days with electronic and room temperature variations), the stroke results are normalized with respect to the voltage range applied, called stroke/voltage gain. The stroke results are shown in Figure 15.

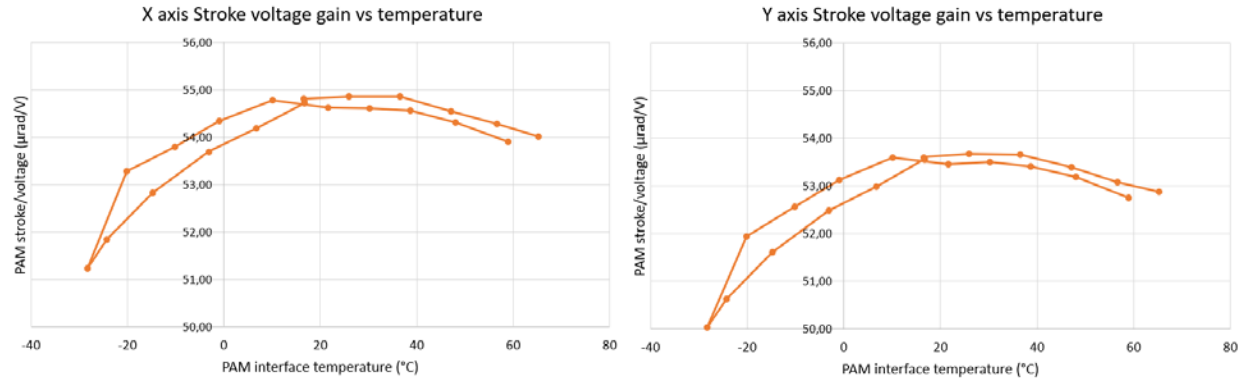

Figure 15. X and Y Stroke/Voltage Gain Through OP Temperature Range – EQM Results

The stroke/voltage gain plot for both axes show the expected bell shape, with a maximum at ambient temperature and loss at cold and hot temperatures. A 7% loss can be seen at -30°C and around 2% loss at +60°C. A conservative 20% and 15% stroke loss was assumed in the design phase (based on past experience on worst cases), explaining the high final stroke margin.

The other noticeable feature is the thermal hysteresis, which should not be there: it is expected for the mechanism to have the same stroke for same temperature (the stroke vs voltage hysteresis observed is however nominal and expected). The reason for this is probably a consequence of the fact PAM temperature was not fully stabilized, tests were performed slightly too quickly after reaching target temperatures and resulted in this thermal hysteresis. The actual temperature data is measured on the PAM support bracket (interface) located under the mechanism, piezo temperatures were not monitored to avoid any potential damage/contamination. Hence it is not possible to directly measure or control piezo temperature.

In order to confirm this thermal delay hypothesis, a simplified thermal-equivalent first order model of the PAM was created, using measured temperature time constants (between PAM interface and the piezos) and a bell-shaped stroke vs temperature look-up table for the piezos.

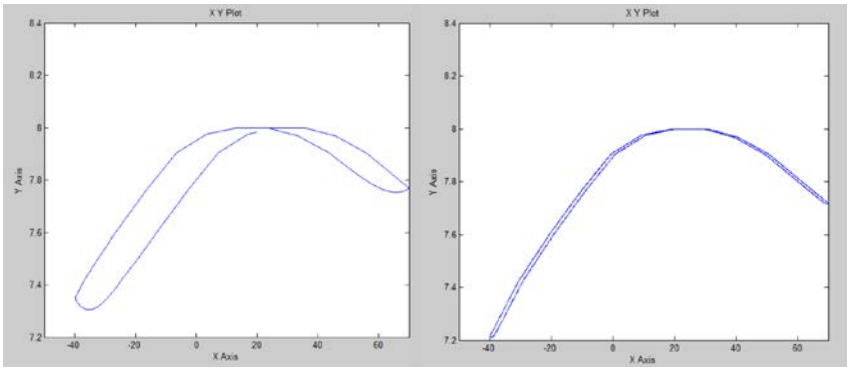

Figure 2. Simplified PAM Thermal Equivalent Model Results (X: Temperature in °C, Y: Stroke in mrad), Left: 10h Cycle Duration (Close to What was Tested), Right: 100h Cycle Duration where Hysteresis is Greatly Reduced.

The model can recreate this hysteretic behavior, which appears to be greatly reduced after greatly increasing thermal stabilization time (x10). However, given that the measurements cannot be automated, an operator has to be there at each step (hence excluding nights and weekends). The EQM test already lasted 3 days and 30 days of testing is not practical. Options to improve the OP Thermal Vacuum Cycle were discussed with the customer.

SG parameters (offset and gain) were also measured for each temperature step, the results for EQM X-axis are shown in Figure 17.

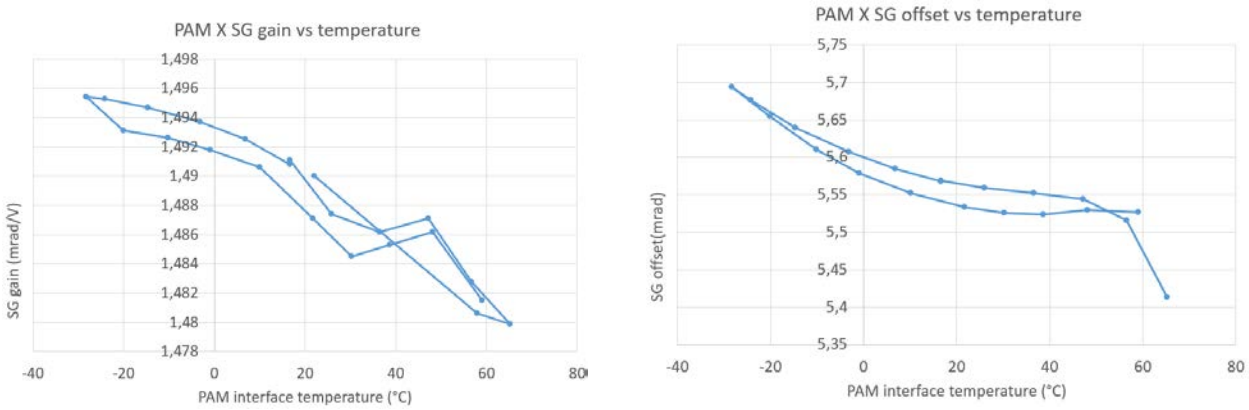

Figure 17. EQM X Axis SG Gain vs Temperature (Left), EQM X Axis SG Offset vs Temperature (Right)

The results are also affected by the piezo temperature delay. As anticipated, the SG gain is quite stable with less than 1% variation through the temperature range. The offset is directly impacted by the mechanism thermomechanical excursion, which was measured at 0.4 mrad total (0.2 to 0.4 mrad on X and Y SG offset).

Vibration Test

All models except EM are planned to go through vibration tests. The tests consist of a random vibration verification as well as a shock test, for each axis. A low-level frequency sweep is performed before and after each test (to assess potential modal landscape changes).

Regarding the random vibration test, the preliminary levels for which the mechanism was analyzed to were 10 grms (20-2000 Hz span with a 50 to 800 Hz 0.08 g^2/Hz plateau). Later in the project, when the updated and refined DSOC full system vibration simulations were performed, the specified levels at PAM interface location had to be increased. The final random vibration levels are much higher and follow the power spectral density (PSD) shown in Table 5.

Table 5. Final PSD for PAM Random Vibration Test

X -Axis Test Spec		Y-Axis Test Spec		Z-Axis Test Spec	
FREQ(Hz)	**ASD(g^2/Hz)**	**FREQ(Hz)**	**ASD(g^2/Hz)**	**FREQ(Hz)**	**ASD(g^2/Hz)**
20	0.100	20	0.1	20	0.1
50	3.500	50	3.5	50	3.5
150	3.500	395	3.5	340	3.5
2000	0.010	2000	0.01	2000	0.01
Grms = 28.03		**Grms = 42.0**		**Grms = 39.5**	

Updated mechanism simulation showed that these new levels remain acceptable, regarding mechanical stress in the parts. The cables and wires, however, were more affected, raising concerns with the updated vibration levels. Wire and cable epoxy staking upgrades are being implemented to mitigate the risk of wire damage, mainly by reducing the free length between tie-down locations.

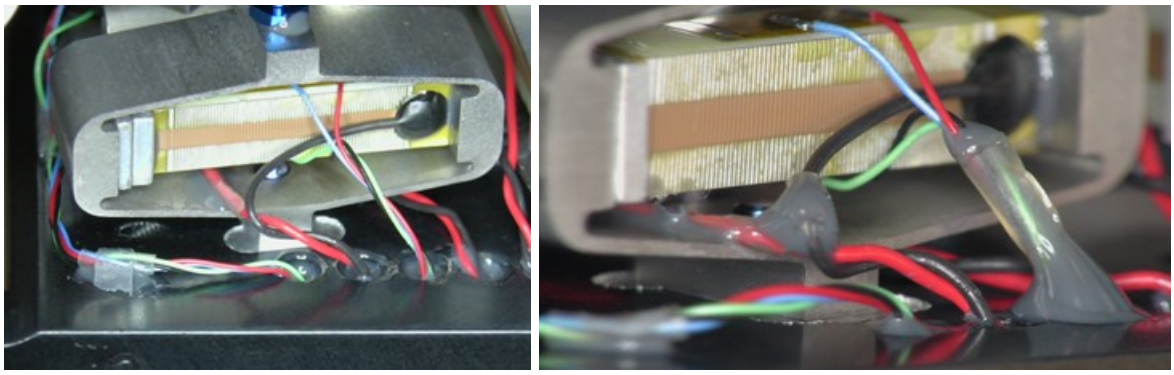

Figure 18. Overview of SG Wires, Initial Configuration (Left) and Reinforced Cabling (Right)

At the time of paper publication, full level vibration tests are planned on a representative model.

Mechanism Delivery Status

At the time of the paper publication, the engineering model (EM) has been delivered. The EQM vibration test is still to be performed for closure of design verification. FM2 acceptance test series has started with thermal vacuum cycling. FM1 was unfortunately irreparably damaged during a subcontracted bake-out failure (decompressive explosion, not implosion, something not expected in a vacuum test), and a new model will be assembled using spare parts and tested.

Conclusion

In this paper, the development, procurement, integration and testing of a novel double tilt PAM mechanism is presented. The mirror integration verification method is explained and the comparison with actual measurements indicate that the results were quite reliable for this case.

The test results now available are presented and indicate that the PAM mechanism is working as intended. Some measurement artifacts on the OP Thermal Vacuum Cycle (thermal hysteresis) were investigated and some improvements will be implemented for incoming FM2 tests.

The upcoming tests are the random vibration and shock with increased levels. The cable wiring is being reinforced in order to ensure the mechanism survival.

Acknowledgment

The authors want to thank all partners involved, among others: Marshall Bernklow and Richard Aigbaeken from L3-Harris-SSG, as well as Dan McDonald and Joseph Kovalik from JPL Optical Communication Laboratory for their support during the project.

References

1. R. Le Letty, F. Barillot, H. Fabbro, F. Claeyssen, Ph. Guay, L. Cadiergues, Miniature Piezo Mechanisms for Optical and Space applications Proc ACTUATOR Conf, Pub. Messe Bremen (G), June 2004, pp 177-180
2. E. Prevost, A. Weickman, S. Belmana, F. Bourgain, O. Sosnicki, F. Claeyssen, Beam Steering Mechanism For Earthcare Atmospheric Lidar Instrument Atlid – An Ultra-Stable Piezoelectric Tip Tilt Mechanism, Proc. ICSO, Biarritz, Oct. 2016
3. F. Claeyssen, T. Maillard, O. Sosnicki, F. Barillot, A.Pages, C.Belly, A.Bataille, M.Logeais, G.Aigouy, T.Porchez, F. Bourgain, Beam Steering Mirrors from space applications to optronic solutions, Proc. OPTRO Conf, Paris, Feb. 2018
4. F. Claeyssen, K. Benoit, G. Aigouy, T.Maillard, M. Fournier, Olivier Sosnicki, Large-Stroke Fast Steering Mirror For Space Free-Space Optical Communication, Proc. OPTRO Conf, Paris, Feb. 2020
5. F. Bourgain, O. Sosnicki, C. Belly, F. Barillot, F. Claeyssen, An Improved Accurate Beam Steering Piezoelectric Mechanism for ATLID Instrument, *Proc. Actuator 2014 Vol.* pp. 293-296
6. T. Mower., Degradation of titanium 6Al-4V fatigue strength due to electrical discharge machining, *International Journal of Fatigue, vol.64, pp 84-96*